Electrocatalysis (2018) 9:505–513
https://doi.org/10.1007/s12678-018-0467-1

ORIGINAL PAPER

Electrocatalytic Behavior of Pd and Pt Nanoislands Deposited onto 4,4′-Dithiodipyridine SAMs on Au(111)

Heiko Müller[1] · Martin Metzler[1] · Natalie Barth[1] · Bert Conings[2] · Hans-Gerd Boyen[2] · Timo Jacob[1] · Ludwig A. Kibler[1]

Published online: 3 April 2018

Abstract

Using different electrochemical techniques as well as in situ scanning tunneling microscopy (STM) and ultraviolet photoelectron spectroscopy (UPS), we investigated the electrocatalytic oxidation of carbon monoxide and methanol on palladium and on platinum nanoislands, which were deposited onto 4,4′-dithiodipyridine self-assembled monolayers (SAMs) on Au(111) single crystal electrodes. Electrochemical and morphological measurements performed on these monoatomic high metal deposits on top of the SAM show rather different island growth along with variations in metal coverage and particle size. UPS He-II valence band spectra of all Pt deposits reveal no intensity at the Fermi energy, so that the resulting nanoislands can be considered as non-metallic. While the electronic and structural properties do not affect carbon monoxide adsorption, the metal coverage has a tremendous impact on the catalytic activity regarding CO oxidation as well as methanol oxidation.

Keywords Electrocatalysis · Self-assembled monolayers · Metallization · CO oxidation · Methanol oxidation

Introduction

Self-assembled monolayers (SAMs) of organothiols and disulfides on metal surfaces have become an essential part in several systems and many devices related to interfacial electrochemistry and surface science [1–5]. The ease of preparation, combined with structural diversity and the possibility to alter the chemical reactivity of the surface by variation of terminal functional groups, makes SAM systems suitable for many applications in nanotechnology. These systems can be used as ultrathin layers for corrosion protection [6, 7], as well as building blocks in sensors and biosensors to immobilize different types of biomolecules (e.g., DNA) [8, 9], and in molecular electronics as transistors and switches [10, 11].

Beyond that, especially metallized SAMs have attracted considerable interest (e.g., in molecular electronics [12] or for rectifiers/transistors [13]) because they offer the prospect of fabricating electronic circuit components for molecular devices [14] on a nanoscale size.

However, so far, only a few methods are available for successful metallization of organic layers [15]. In the particular case of thiol or dithiol SAMs on gold electrodes, the existence of well-ordered structures is advantageous for metallization [4]. Thus, an applicable method for the metallization of SAM-modified gold surfaces is electroless deposition, which is referred to as forced deposition by using reducing agents dissolved in the electrolyte [16, 17]. The utilization of hydrogen as reducing agent ensures the absence of possible impurities in the final metal deposit [18]. Alternatively, various SAM metal junctions can be prepared by simple electrochemical techniques [19, 20]. Ideal combinations involve aromatic molecules (e.g., 4-mercaptopyridine, 4,4′-dithiodipyridine, 4-aminothiophenol, thiazole, 1,4-dicyanobenzene) and noble metals such as Pd, Pt, and Rh [19, 21–28]. Interestingly, the formation of a molecular "double-decker" showed an extension of this method to even obtain 3D architectures [29]. A well-ordering of the SAM structures seems to be mandatory for simple metallization in order to obtain monoatomic high metal islands of nanometer size. In addition, chemical functionalization, e.g., via the nitrogen of the pyridine ring

Electronic supplementary material The online version of this article (https://doi.org/10.1007/s12678-018-0467-1) contains supplementary material, which is available to authorized users.

✉ Ludwig A. Kibler
ludwig.kibler@uni–ulm.de

[1] Institut für Elektrochemie, Universität Ulm, 89069 Ulm, Germany

[2] Institute for Materials Research (IMO-IMOMEC), Hasselt University, 3590 Diepenbeek, Belgium

in 4-mercaptopyridine (4-PyS) facing the electrolyte side, is crucial for a successful metallization, since it was shown that metallization of thiophenol and 2-mercaptopyridine (both with no nitrogen being directly oriented towards the electrolyte) could not be achieved [26, 27]. It is assumed that molecular complexes of noble metal cations with the adsorbed 4-mercaptopyridine ligands are formed prior to the deposition step. The SAM molecules were found to adsorb via the thiolate group in threefold hollow sites on the Au(111) surface, which results in an ordered ($\sqrt{3} \times \sqrt{3}$) superstructure for saturation coverage as shown by theoretical calculations [30, 31]. For simplicity, it was therefore assumed earlier that the 4-mercaptopyridine coverage equals 1/3 with respect to the Au(111) surface atoms in agreement with these theoretical calculations. However, more precisely, under the typical electrochemical conditions, lower coverages of the 4-mercaptopyridine SAM with ($5 \times \sqrt{3}$) and ($7 \times \sqrt{3}$) structures have been observed [21, 22]. Furthermore, the experimental SAM structures are strongly dependent on the applied electrode potential (transition from ordered to disordered structures), nature of the electrolyte as well as the adsorbed anions (perchlorate vs. (bi)sulfate), pH of the electrolyte, and finally the source of the adsorbed molecules itself (4-mercaptopyridine compared to 4,4′-dithiodipyridine) [21, 22, 32–35].

Since metallized SAMs have been investigated in great detail in the past with respect to their formation and morphological properties [19, 23–27, 36], the resulting nanoscaled metal islands can now serve as attractive platforms to study their electrocatalytic behavior, as island size and electronic structure can be tuned over a wide range.

In the present work, the electrocatalytic properties of monoatomic high Pd and Pt nanoislands deposited onto 4,4′-dithiodipyridine on Au(111) are studied as a function of metal loading, the electronic nature of the metal as well as the size of the nanoislands. While massive Pd and Pt electrodes are well known as active catalysts for the oxidation of small molecules such as CO, methanol, and formic acid, appropriate nanoislands formed on a SAM-modified Au(111) electrode provide the opportunity to investigate systems that differ from both bulk metal and metal clusters, respectively.

In our experiments, 4,4′-dithiodipyridine (4-PySSPy) was used, which is known to form a ($7 \times \sqrt{3}$) superstructure in sulfuric acid at 0.2 monolayer coverage. This SAM system has been investigated in great detail and shows reproducible structures and coverage [19, 22, 26–28]. Metallization of the thus formed 4,4′-dithiodipyridine SAM with either Pd or Pt was achieved by spontaneous binding metal complexes to the pyridine nitrogen groups and subsequent electrochemical reduction in electrolytes free of metal salt [19, 26, 27]. As confirmed by angle-resolved X-ray photoelectron spectroscopy (AR-XPS) earlier, this procedure enables the deposition of both metals on top of the SAM rather than onto the Au(111) substrate itself [19, 27, 29]. Furthermore, photoemission spectroscopy using He-II radiation (UPS) allowed to extract valuable information about the electronic properties in the case of Pd islands in the past, thereby identifying a non-metal to metal transition as function of metal coverage [36]. Consequently, in the present study, additional UPS measurements have been performed on Pt islands, allowing for a direct comparison of electronic properties between both metal overlayer systems. These measurements have been complemented by extensive morphological (in situ STM) and electrocatalytic characterizations.

Experimental

The Au(111) electrode (MaTecK, Jülich, Germany) used for electrochemical measurements was a cylinder (0.4 cm diameter, 0.125 cm^2 surface area) with one of its faces oriented to better than 1°. Before each experiment, the electrode was prepared by flame annealing and subsequent cooling in a nitrogen atmosphere. The samples were prepared by combining currentless and electrochemical methods, following the approach of Kolb and co-workers [19]. The freshly annealed Au(111) electrode was immersed for 10 min without potential control into an aqueous solution of 20 μM 4,4′-dithiodipyridine, which was deaerated to prevent oxidation of the disulfide molecules. After rinsing the thiol-modified electrode with ultrapure water, the sample was immersed into a metal-ion-containing solution (0.1 mM $PdSO_4$ or $K_2[PtCl_4]$) for 5 or 15 min, respectively. After rinsing thoroughly with ultrapure water, the electrode was transferred into a metal-ion-free electrochemical cell, where it was contacted at 0.5 V vs. SCE with 0.1 M H_2SO_4 to prevent immediate reduction of the adsorbed metal ions. Afterwards, the adsorbed metal ions were reduced electrochemically. Subsequently, the prepared samples were rinsed again with ultrapure water and transferred to another reaction solution containing electrochemical cell (0.1 M H_2SO_4 or 0.1 M NaOH + 2.5 M MeOH), where they were contacted at negative potential with the electrolyte to prevent the adsorption of anions or unintentional oxidation of the reaction species. For the CO oxidation experiments, CO was bubbled into the electrolyte for at least 10 min. Before CO stripping, the electrolyte was purged with nitrogen to remove dissolved CO from solution.

The solutions were made of H_2SO_4 (Merck, Suprapur), 4,4′-dithiodipyridine (Acros Organics, 98%, as received), $PdSO_4$ H_2O (Alfa Aesar, 99.95%), K_2PtCl_4 (Aldrich, 99.99%), MeOH (Fluka, 99.9%), NaOH × H_2O (Merck, 99.99%), and ultrapure water (18.2 MΩ cm, TOC <3 ppb) which was deaerated with nitrogen 5.0 (MTI) or argon 5.0 (MTI). All experiments were carried out at room temperature with a standard electrochemical setup and a saturated calomel

electrode (SCE, Schott, B 3510) as reference electrode. All potentials are given with respect to SCE.

The in situ scanning tunneling microscopy (STM) experiments were performed with a Topometrix TMX 2010 Discoverer STM. A larger Au(111) electrode with a diameter of 12 mm (MaTecK) was used for STM measurements because of cell design. The preparation of the electrode and the samples is similar to the one described for the electrochemical measurements. The electrode was brought in contact with the electrolyte in the STM cell under potential control. A high-purity Pt wire (Götze, 99.995%) served as quasi-reference electrode. The tunneling tips used in the experiments were etched from Pt/Ir (80/20) wires (MaTecK, 99.99%) coated with electrophoretic paint (BASF) to minimize Faraday currents at the foremost part of the tip. All images were recorded in the constant-current mode ($I_t = 1$ nA).

Further details about the experimental approach as well as the experimental setup for cyclic voltammetry and in situ STM can also be found in literature [19, 21, 26].

To guarantee a high quality of the samples and to exclude the presence of contaminations, their chemical states were analyzed by means of XPS performed on a commercial photoemission system (PHI-5600LS), offering monochromatized X-rays (1486.6 eV) for photoionization. The electronic structure of the Pt islands was studied using UPS carried out with non-polarized He-II radiation (40.8 eV) as provided by a gas discharge lamp. The binding energy scale of the instrument was calibrated by means of an independent Au reference sample, thereby setting the Au-4$f_{7/2}$ binding energy position to 84.0 eV.

Results and Discussion

The Pd and Pt islands are prepared by consecutive deposition cycles onto a 4-PyS SAM that is formed by dissociative adsorption of 4-PySSPy on Au(111) [22, 26]. A so-called deposition cycle includes complexation of the metal complex with the pyridine groups of the SAM and subsequent selective electrochemical reduction, a process that can be done repeatedly to achieve coverages of between 0.2 (single complexation step) and 0.95 ML (multiple complexation steps).

The structure of the nanoislands has been investigated in detail by in situ STM measurements (Fig. 1). While metal ions are localized at the pyridine nitrogen, after the reduction, continuous metal islands are formed (Fig. 1). Although one might expect that the reduced metal atoms might diffuse through the relatively open SAM layer and adsorb onto the Au surface, theoretical calculations have shown that Pd water complexes are formed so that they remain on top of the SAM layer [30]. Further, barrier heights for lateral diffusion steps of Pd atoms on top of a 4-PyS SAM with pre-adsorbed palladium atoms are low enough to facilitate the observed island formation [30]. After the first deposition cycle, the nanoislands are monoatomic high (Fig. S1a–d) and have diameters between 3 and 12 nm (Fig. 1a, c). Already in the case of a single palladium deposition cycle, the 4-mercaptopyridine adlayer is not ordered anymore. Only for very low Pt coverages (large separation between the islands), the long-range ordering of the SAM is retained [27]. The presence of Pd and Pt nanoislands seems to destabilize the previously ordered SAM structure. The Pt islands are quite uniform in size and shape, whereas Pd shows larger variation of size and nanoislands of different shape. An increase in metal coverage by repeated deposition leads to an increase of homogenously distributed Pt islands while Pd rather forms larger, coalescing islands that grow up to an almost full monolayer after three deposition cycles (Fig. 1b, d). For both metals, bilayers are partially formed during the third deposition cycle.

So far, a maximum platinum coverage of about 0.45 ML has been observed after three consecutive deposition cycles (Fig. 1d). In addition to the formation of two-dimensional islands, metal atoms in the second layer can partly be observed in Fig. 1b, d.

Figure 2 shows the coverage of Pd and Pt as function of the number of cycles for complexation and subsequent electrochemical reduction. In the following, the numbers of these metal deposition cycles are denoted as #1–3. The metal coverage was determined from the cathodic charge density for electrochemical deposition (Fig. S2) and was compared with in situ STM images (cf. Fig. 1). Considering that after each single deposition cycle the number of free pyridine nitrogen sites for subsequent complexation decreases, the dashed curves represent the expected metal coverage. The experimental values can differ from this expected trend due to additional influences such as surface morphology (e.g., partial growth of 2nd monolayer) and the number of metal atoms per surface area (lattice spacing). For a complete metal monolayer deposited onto the SAM on an Au(111) substrate, the charge density for electrochemical deposition is equivalent to 444 μC cm^{-2}. On the other hand, the metal coverage determined from in situ STM images is obtained by comparing the integral area formed by the metal islands to the total surface area of the gold support. In the absence of atomic resolution, structures pseudomorphic with that of Au(111) are assumed for the metal islands. The morphological parameters extracted for both types of nanoislands (Pd or Pt) after the different complexation/reduction cycles are summarized in Table 1, together with an evaluation of their metallicity (see below). Binding of a single metal ion per pyridine nitrogen fits well to the metallization with Pt, since the coverage of 4-mercaptopyridine equals 0.2 ML. For the Pd system, even two metal ions per pyridine nitrogen are present. Nevertheless, an almost complete palladium monolayer can be fabricated by repeated deposition cycles, because palladium grows on a surface with already existing islands [26].

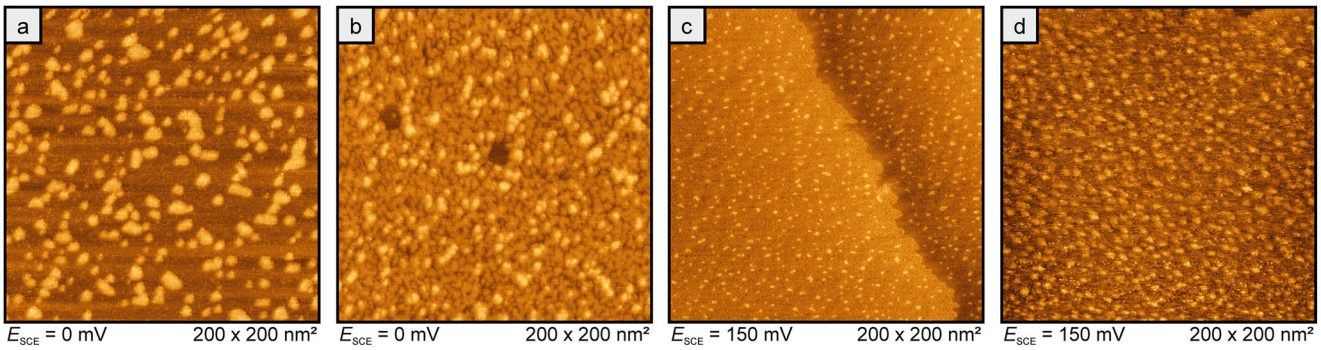

Fig. 1 In situ STM images in 0.1 M H_2SO_4 of 4-mercaptopyridine SAM on Au(111) after the deposition of metal islands: **a** 0.33 ML Pd, **b** 0.95 ML Pd, **c** 0.18 ML Pt, and **d** 0.45 ML Pt.

Although, the different behavior in metal coverage can be related to the nature of the metal salt ($[Pd(H_2O)_4]^{2+}$ vs. $[PtCl_4]^{2-}$), using the $[PdCl_4]^{2-}$ complex for metallization unexpectedly leads to the same metal coverage of the Pd(II) aquo complex (not shown here).

Surprisingly, 4-mercaptopyridine was recently found to enhance the electrocatalytic activity of formic acid oxidation on Au(111). Therefore, at first, the catalytic activity of the 4-PyS SAM on Au(111) that anchors the nanoislands was investigated for the CO oxidation reaction to make sure that the electrocatalytic properties of the nanoislands are established without significant contributions arising from the SAM itself. Figure 3 presents a current-potential curve for a 4-PyS-modified Au(111) surface in sulfuric acid in its stability range between −0.2 and 0.9 V. At more negative potentials, the reductive desorption of the SAM starts, while at more positive potentials, the oxidative desorption of the SAM takes place.

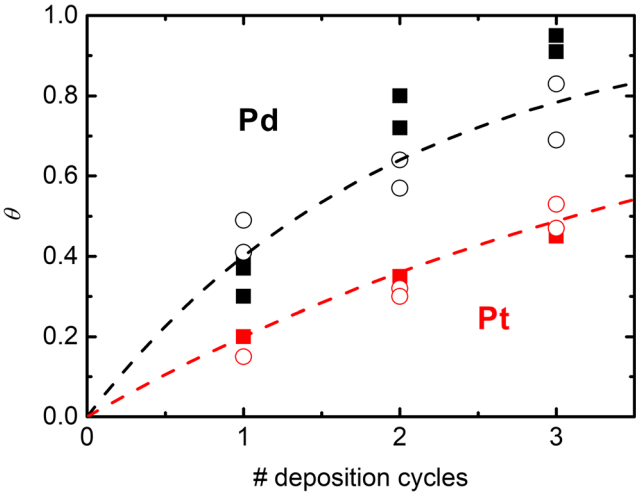

Fig. 2 Coverage of Pd (black symbols) and Pt (red symbols) as a function of the number of complexation/reduction cycles, determined by in situ STM (filled symbols) as well as by taking the deposition charge densities into account (open circles). Considering that after each single deposition cycle the amount of free pyridine nitrogen for subsequent complexation decreases, the dashed curves represent the theoretically expected metal coverage

The peak at 0.38 V indicates sulfate adsorption accompanied by an order–disorder transition within the SAM structure. A current-time measurement during CO bubbling for 10 min at 0.2 V showed no significant current and the subsequent cyclic voltammogram revealed no indication for CO bulk oxidation on the 4-PyS-modified Au(111) surface. While Au(111) is a poor catalyst for CO oxidation under certain conditions (additional nitrogen flow), the SAM structure is completely inactive for CO oxidation. This is advantageous for studying the electrocatalytic behavior of metal nanoislands only in terms of the metal species as well as the electronic character and size of the islands.

An applicable method for investigating the electrocatalytic behavior and nature of the metal nanoislands is to measure their interaction between a metal and a specific adsorbate such as CO, which is an important reactant for many reactions in electrocatalysis and a structure-sensitive probe molecule. The current-potential curves for CO bulk oxidation on palladium- and platinum-metallized 4-PyS SAM on Au(111) in 0.1 M H_2SO_4 are shown in Fig. 4a, b, demonstrating that the metal islands indeed possess electrocatalytic activity for the oxidation of small molecules, even if the pure 4-PyS SAM itself is inactive. It is obvious that at higher metal coverages (Pt 0.45 ML), platinum is more active, as revealed by significant higher currents and an onset potential for CO oxidation that is considerably more negative than that of palladium (Pt 0.2 V, Pd 0.4 V). This difference in electrocatalytic activity is even more obvious taking into consideration the lower platinum coverage (compared to the Pd system, 0.95 ML) (cf. Fig. 2). As a systematic increase in activity for CO bulk oxidation relative to the metal loading can be observed for palladium, this is noteworthy higher for platinum islands with larger diameter, which is indicative of a change in the electronic properties. This is also evident from the mass activity curve of CO bulk oxidation at +0.6 V against the metal coverage, where the activity per metal atom is increased drastically for higher coverages (Fig. 4c). It has to be mentioned that CO bulk oxidation overlaps with the palladium oxidation/dissolution. Therefore, an excursion to more positive potentials could

Table 1 Coverages θ, average island diameter d, and metallicity of the Pd and Pt deposits relative to their number of complexation/reduction cycles

Material	# complexation	θ_{theo}/ ML	θ_{CV}/ ML	θ_{STM}/ ML	d_{island}/ nm	Metallicity
Pd	1	0.40	0.41	0.37	10	Non-metallic [36]
	2	0.64	0.69	0.72	—*	Metallic [36]
	3	0.78	0.83	0.91	—*	Metallic
Pt	1	0.20	0.15	0.20	4	Non-metallic
	2	0.36	0.30	0.35	8	Non-metallic
	3	0.49	0.47	0.45	8	Non-metallic

*No determination of the average island diameter because of the coalescing islands after the 2nd and 3rd complexation

destroy these SAM metal junctions. Furthermore, the choice of electrolyte has an important influence on the electrocatalytic activity, since a non-specific adsorbing anion, such as perchlorate, results in an at least threefold higher activity due to the absence of specifically adsorbing and blocking anions on the surface.

In addition to CO bulk oxidation, CO adlayer oxidation has been studied on the metal islands with variable coverage, size, and metallic character. Figures 5a and 6a exemplarily show current-potential curves on threefold metallized 4-PyS-modified Au(111) surfaces in 0.1 M H_2SO_4 with adsorbed CO. CO adlayer oxidation on platinum islands leads to a coverage of adsorbed CO that increases linearly with the platinum coverage, but is half the CO coverage in comparison to a Pt(111) electrode. This means that the amount of adsorbed CO is determined by the total amount of platinum deposited on the SAM, regardless of the possible changes in the electronic structure or changes in island size. An explanation for the difference to bulk metal can be related to weaker binding of CO (or a different adsorption/desorption equilibrium).

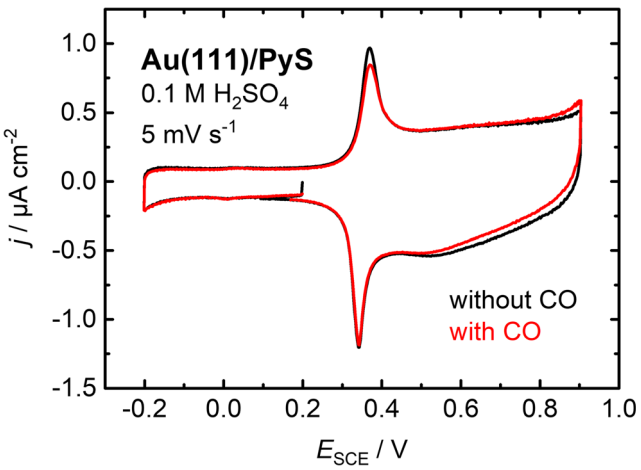

Fig. 3 Current-potential curves for 4-PyS-modified Au(111) in 0.1 M H_2SO_4 with and without CO in electrolyte. Scan rate 5 mV s^{-1}

$$H_2O_{(l)} \rightarrow OH_{ad} + H^+_{(aq)} + e^-$$
$$CO_{ad} + OH_{ad} \rightarrow CO_2 + H^+_{(aq)} + e^-$$
$$\theta_{CO} = \frac{Q_{CO}}{2\,Q_{SA}}$$

Here, Q_{CO} and Q_{SA} are the charge densities for oxidation of the adsorbed CO layer as well as the charge density for one electron transferred per surface atom, respectively. For simplicity, anion influences are ignored.

The platinum coverage was determined by the charge of the reductive deposition cycles after various repetitive complexation and deposition steps. The CO coverage could be estimated by the oxidation of irreversibly adsorbed CO, assuming that CO oxidation involves two electrons. Carrying out the same analytical method for the determination of the maximum possible adsorbed CO coverage on Pt(111), a freshly prepared Pt(111) electrode is the starting point from which we extrapolate the latter for lower platinum coverage depicted in the red curve of Fig. 5b.

CO adlayer oxidation cannot easily be quantified for Pd due to the limited stability of the system, as extending the potential limit causes dissolution of the palladium islands (Fig. 6a, b). The voltammetric peak in the negative scan at around 0.5 V is characteristic for subsequent palladium deposition onto the Au(111) surface and underneath the SAM, respectively. Another indication for small amounts of palladium on the Au(111) surface is the beginning of hydrogen absorption, which has not been observed for SAM metal junctions where the palladium is on top of the SAM. The release of absorbed hydrogen can be observed as a small hump at −0.2 V.

Furthermore, the oxidation of methanol with several different reaction pathways serves as an ideal electrocatalytic reaction to gain more insights into the kinetics and necessity of co-adsorbates such as OH_{ad} on the reaction properties of the nanoislands. Figure 7a shows the current-potential curves for differently prepared Au(111) in 0.1 M NaOH. The adsorption of OH already starts at negative potentials, which is in good agreement with other measurements such as cyclic voltammetry, differential capacity, chronocoulometry, and Fourier transform infrared spectroscopy [37]. The peak at 0.1 V before the onset of the surface oxidation at 0.2 V is associated with the lifting of the surface reconstruction. The surface reconstruction of Au(111) is lifted at the early stages of OH adsorption or oxide formation [38, 39]. OH adsorption on Au(111) is blocked by the adsorbed SAM (red curve). In addition, the stability region is extended because the characteristic peak for monolayer oxidation of gold was not observed. The metallized SAM shows a similar stability region, but without any indication of OH adsorption. On bare Au(111), the methanol oxidation occurs at potentials where OH is adsorbed on the surface and where the gold oxide starts forming. Davis et al.

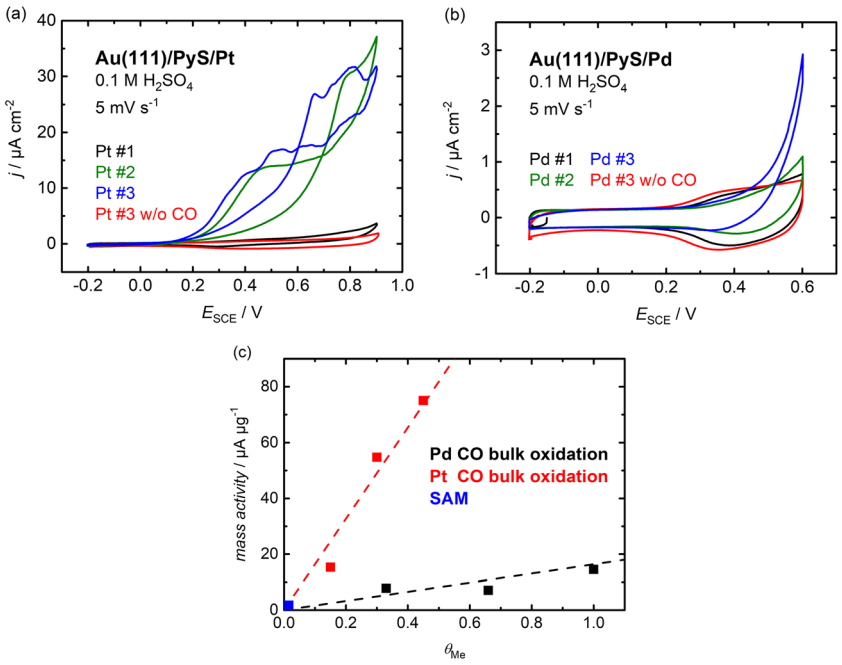

Fig. 4 Current-potential curves for CO bulk oxidation on Pt- (**a**) and Pd- (**b**) metallized 4-PyS-modified Au(111) in 0.1 M H_2SO_4. Scan rate 5 mV s^{-1}. **c** Plot for mass activity of CO bulk oxidation at + 0.6 V plotted against the coverage of Pt (red symbols) and Pd (black symbols)

suggested that the reaction path of alcohol oxidation involves both solution-mediated and metal-catalyzed elementary steps [40], so that OH in solution could be more important for the overall reactivity than OH bound to the gold catalyst [41].

First of all, there is no sign for methanol oxidation on the SAM-modified Au(111) surface. The SAM molecules seem to prevent the necessary OH adsorption on the gold surface by blocking active sites (red curve Fig. 7c). Although the stability region is limited to a positive potential of 0.3 V, a distinct increase in activity for methanol oxidation on the metallized SAM can be observed, since the onset of the latter has a constant shift to more negative potentials. At first sight, the activity for methanol oxidation on the metal nanoislands is lower than on bare Au(111) (Fig. 7b). Indeed, as is the case of CO oxidation, the size and the surface coverage of the islands affect their electrocatalytic behavior significantly. With the exception of the lowest palladium coverage, where barely any activity could be detected, the mass activity behavior demonstrates an increased activity per metal atom for higher coverages (Fig. 7d). Current-time measurements (not shown here) in the region of methanol oxidation at 0.05 V show a steady decrease in current. A possible reason can be poisoning of the surface by CO, which is one of the reaction products. Nevertheless, considering that there are indications of a weaker binding of CO compared to bulk metal, it is possible that the metal islands are less easily poisoned. So far, these measurements are preliminary results that pave the way for forthcoming studies on CO oxidation in 0.1 M NaOH on the metallized 4-PyS SAM to discuss, e.g., the poisoning of the nanoislands in more detail.

Combining now the results presented in Figs. 4 and 7, it becomes clear that for both metal overlayer systems, the electrocatalytic activity depends strongly (linearly) on the metal coverage but not necessarily on the island size. This becomes even more clear when analyzing the results summarized in Table 1: here, the same Pt island size (8 nm) is observed after the second and third deposition cycle, while the highest activity is detected for both catalytic reactions (Figs. 4 and 7) only after the third deposition step.

To investigate whether or not the catalytic activities are influenced by electronic properties, such as the metallicity of the nanoislands, additional UPS measurements were

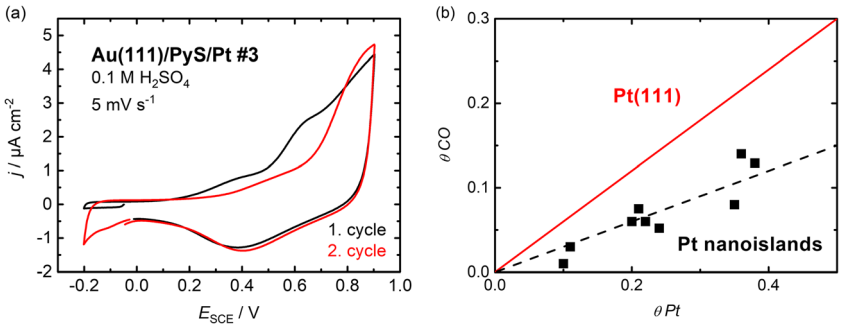

Fig. 5 **a** Current-potential curves for CO adlayer oxidation on three times Pt-metallized 4-PyS-modified Au(111) in 0.1 M H_2SO_4. Scan rate 5 mV s^{-1}. **b** CO coverage plotted against the Pt coverage determined by reductive charge of current-potential curves or graphic analysis of in situ STM images

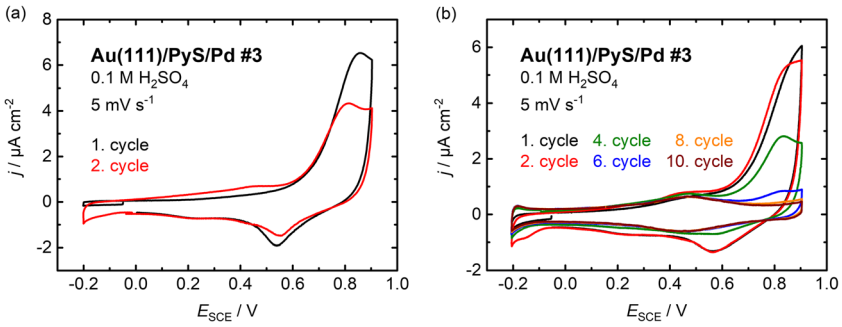

Fig. 6 **a** Current-potential curves for CO adlayer oxidation on Pd-metallized 4-PyS-modified Au(111) in 0.1 M H_2SO_4. Scan rate 5 mV s^{-1}. **b** Current-potential curves for three times Pd-metallized 4-PyS-modified Au(111). Scan rate 5 mV s^{-1}. Pd oxidation due to small stability region

performed after the different deposition cycles in the case of Pt. A similar study of Pd nanoislands was reported earlier [36]. There, UPS measurements combined with density functional theory calculations of palladium nanoislands revealed a non-metal to metal transition with increasing metal coverage. While no metallic character is found for the lowest coverage of the Pd nanoislands, the measurements for an almost closed palladium monolayer on the SAM reveal a significant density of states (DOS) at the Fermi level E_F. Figure 8 now summarizes the UPS He-II valence band spectra obtained with very high surface sensitivity (information depth of few atomic layers only) from the different metallized Pt samples, after subtracting the contribution arising from the support (measured before metallization under identical conditions), in comparison to a clean Pt bulk reference sample. Three characteristic features can be recognized at binding energies E_B of 2.1, 2.6, and 3.1 eV, which are common to all three deposition cycles but which differ significantly from the bulk Pt spectrum. The latter clearly shows a high intensity at the Fermi energy ($E_B = 0$), which is absent for the Pt nanoislands independent of their size (see Table 1). Consequently, for all Pt deposition cycles, the resulting nanoislands can be considered as non-metallic. This contrasts the behavior of Pd islands where a size-induced non-metal/metal transition in the electronic density of states was found arising from the coalescence of individual islands into bigger aggregates at a coverage of about 0.7 ML. As coalescence does not occur for Pt overlayers even after the third deposition cycle, a non-metallic behavior with vanishing density of states at the Fermi level is expected for all three Pt depositions, in perfect agreement with the experimental results shown in Fig. 8.

Combining now the results obtained for both metal systems, there is clear evidence that the observed electrocatalytic activities neither scale with the island size nor depend strongly on the electronic density of states at the Fermi level, but are exclusively linked to the achieved surface coverage. This is a rather surprising result, as chemical reactivities of a system are often controlled by its local electronic structure, as found for nanoscaled systems such as atomic clusters or bulk surfaces with local defects and steps.

Metallized 4-PyS SAMs show an enhanced activity for formic acid oxidation compared to bare Au(111).

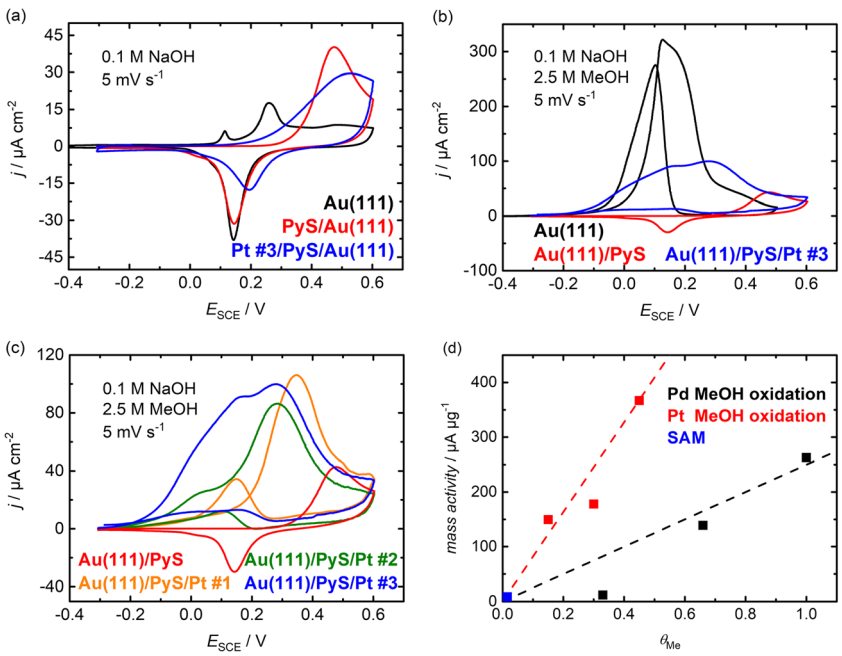

Fig. 7 Current-potential curves for differently prepared Au(111) in 0.1 M NaOH (**a**) and in 0.1 M NaOH + 2.5 M MeOH (**b**, **c**). Scan rate 5 mV s^{-1}. **d** Mass activity for MeOH oxidation at 0.1 V plotted against the coverage of Pt (red symbols) and Pd (black symbols)

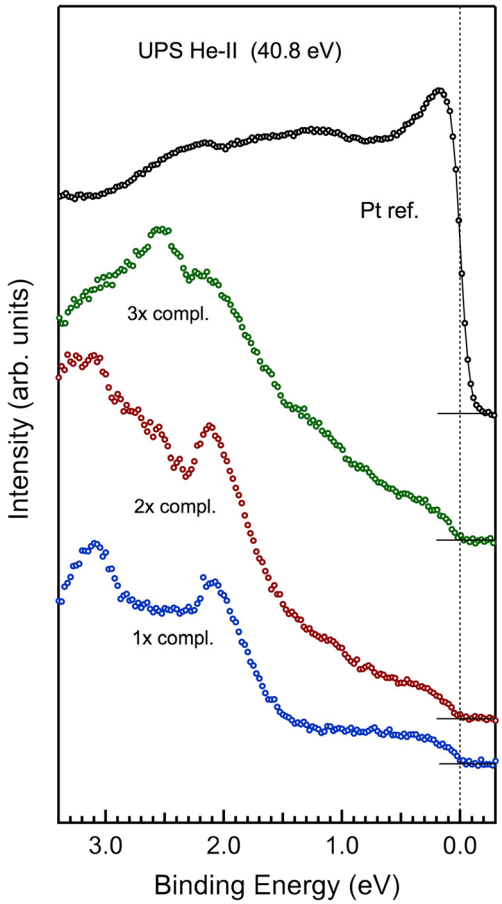

Fig. 8 UPS spectra acquired from different Pt-covered samples after subtracting the contribution due to the support, thus only representing the properties of the Pt overlayers. The results measured on a clean Pt reference sample have been added for comparison

Interestingly, the activity of the 4-PyS-modified Au(111) surface before metal deposition is five times higher than that of the nanoislands. Structure and configuration of the SAM as well as pH and the applied potential are important for this altered activity. It appears that the nanoislands on the SAM just inhibit changes in its structural configuration.

Conclusion

The electrocatalytic behavior of Pd and Pt nanoislands deposited onto 4,4′-dithiodipyridine SAMs on Au(111) has been studied using CO and methanol oxidation as reference reactions. The structural and electronic properties of the nanoislands have been investigated by electrochemical techniques, in situ STM, and photoelectron spectroscopy. We analyzed the variation of metal coverage, particle size, and metallic character as function of the number of complexation and subsequent electrochemical deposition steps, and their impact on the electrocatalytic behavior of platinum and palladium nanoislands. Although the SAM as a spacer and anchoring molecule is not catalytically active itself, it enables the necessary electron transfer through the SAM. While CO and methanol oxidation can be performed for both Pd and Pt islands, the higher activity per atom as well as the larger electrochemical window makes Pt nanoislands particularly advantageous for electrocatalytic oxidation. While the SAM-covered Au(111) surface is catalytically inactive, the electrocatalytic activity of the Pt nanoislands for CO and methanol oxidation increases with increasing coverage. The adsorption of CO on the nanoislands seems to be weaker compared to adsorption on the bulk metal, which can be favorable for a catalyst to be less susceptible to surface poisoning. While the electronic and dimensional properties of the nanoislands have no effect on the ability to adsorb CO, it seems that only the metal coverage itself is the main factor determining the electrocatalytic activity.

Acknowledgements The authors thank Claus Müller for his technical STM support.

Funding Information Financial support has been received from the Deutsche Forschungsgemeinschaft (DFG) through the grant KO 576/28-1.

References

1. R.G. Nuzzo, D.L. Allara, Adsorption of bifunctional organic disulfides on gold surfaces. J. Am. Chem. Soc. **105**(13), 4481–4483 (1983)
2. L.H. Dubois, R.G. Nuzzo, Synthesis, structure, and properties of model organic surfaces. Annu. Rev. Phys. Chem. **43**(1), 437–463 (1992)
3. A. Ulman, Formation and structure of self-assembled monolayers. Chem. Rev. **96**(4), 1533–1554 (1996)
4. J.C. Love, L.A. Estroff, J.K. Kriebel, R.G. Nuzzo, G.M. Whitesides, Self-assembled monolayers of thiolates on metals as a form of nanotechnology. Chem. Rev. **105**(4), 1103–1170 (2005)
5. C. Vericat, M.E. Vela, G. Benitez, P. Carro, R.C. Salvarezza, Self-assembled monolayers of thiols and dithiols on gold: new challenges for a well-known system. Chem. Soc. Rev. **39**(5), 1805–1834 (2010)
6. O. Azzaroni, M. Cipollone, M.E. Vela, R.C. Salvarezza, Protective properties of dodecanethiol layers on copper surfaces: the effect of chloride anions in aqueous environments. Langmuir **17**(5), 1483–1487 (2001)
7. G. Brunoro, A. Frignani, A. Colledan, C. Chiavari, Organic films for protection of copper and bronze against acid rain corrosion. Corros. Sci. **45**(10), 2219–2231 (2003)
8. R. Levicky, T.M. Herne, M.J. Tarlov, S.K. Satija, Using self-assembly to control the structure of dna monolayers on gold: a neutron reflectivity study. J. Am. Chem. Soc. **120**(38), 9787–9792 (1998)
9. B. Bonanni, A.R. Bizzarri, S. Cannistraro, Optimized biorecognition of cytochromec551 and azurin immobilized on thiol-terminated monolayers assembled on Au(111) substrates. J. Phys. Chem. B **110**(30), 14574–14580 (2006)
10. J.M. Tour, Molecular electronics. Synthesis and testing of components. Acc. Chem. Res. **33**(11), 791–804 (2000)
11. T. Sugawara, M.M. Matsushita, Spintronics in organic π-electronic systems. J. Mater. Chem. **19**(12), 1738–1753 (2009)
12. J.M. Seminario, Approaching reality. Nat. Mater. **4**(2), 111–113 (2005)

13. G. Cuniberti, G. Fagas, and K. Richter, in Introd. Mol. Electron. (Lecture Note Physics), edited by G. Cuniberti, K. Richter, G. Fagas (Springer Berlin, Berlin, 2005), pp. 1–10
14. J.M. Seminario, J.M. Tour, Ab initio methods for the study of molecular systems for nanometer technology: toward the first-principles design of molecular computers. Ann. N. Y. Acad. Sci. **852**(1 MOLECULAR ELE), 68–94 (1998)
15. H. Haick, D. Cahen, Making contact: connecting molecules electrically to the macroscopic world. Prog. Surf. Sci. **83**(4), 217–261 (2008)
16. H. Kind, A.M. Bittner, O. Cavalleri, K. Kern, T. Greber, Electroless deposition of metal nanoislands on aminothiolate-functionalized Au(111) electrodes. J. Phys. Chem. B **102**(39), 7582–7589 (1998)
17. E.A. Speets, P. Te Riele, M.A.F. Van Den Boogaart, L.M. Doeswijk, B.J. Ravoo, G. Rijnders, J. Brugger, D.N. Reinhoudt, D.H.A. Blank, Formation of metal nano- and micropatterns on self-assembled monolayers by pulsed laser deposition through nanostencils and electroless deposition. Adv. Funct. Mater. **16**(10), 1337–1342 (2006)
18. M.I. Muglali, A. Bashir, A. Birkner, M. Rohwerder, Hydrogen as an optimum reducing agent for metallization of self-assembled monolayers. J. Mater. Chem. **22**(29), 14337–14340 (2012)
19. T. Baunach, V. Ivanovo, D.M. Kolb, H.-G. Boyen, P. Ziemann, M. Büttner, P. Oelhafen, A new approach to the electrochemical metallization of organic monolayers: palladium deposition onto a 4,4′-dithiodipyridine self-assembled monolayer. Adv. Mater. **16**(22), 2024–2028 (2004)
20. I. Thom, G. Hähner, M. Buck, Replicative generation of metal microstructures by template-directed electrometallization. Appl. Phys. Lett. **87**(2), 024101 1–3 (2005)
21. T. Baunach, V. Ivanova, D.A. Scherson, D.M. Kolb, Self-assembled monolayers of 4-mercaptopyridine on Au(111): A potential-induced phase transition in sulfuric acid solutions. Langmuir **20**(7), 2797–2802 (2004)
22. W. Zhou, T. Baunach, V. Ivanova, D.M. Kolb, Structure and electrochemistry of 4,4‘-dithiodipyridine self-assembled monolayers in comparison with 4-mercaptopyridine self-assembled monolayers on Au(111). Langmuir **20**(11), 4590–4595 (2004)
23. M. Manolova, H.-G. Boyen, J. Kucera, A. Groß, A. Romanyuk, P. Oelhafen, V. Ivanova, D.M. Kolb, Chemical interactions at metal/molecule interfaces in molecular junctions—a pathway towards molecular recognition. Adv. Mater. **21**(3), 320–324 (2009)
24. F. Eberle, M. Kayser, D.M. Kolb, M. Saitner, H.-G. Boyen, M. Dolieslaeger, D. Mayer, A. Wirth, Metallization of organic surfaces: Pd on thiazole. Langmuir **26**(7), 4738–4742 (2010)
25. F. Eberle, M. Metzler, D.M. Kolb, M. Saitner, P. Wagner, H.-G. Boyen, Metallization of ultra-thin, non-thiol SAMS with flat-lying molecular units: Pd on 1, 4-dicyanobenzene. ChemPhysChem **11**(13), 2951–2956 (2010)
26. V. Ivanova, T. Baunach, D.M. Kolb, Metal deposition onto a thiol-covered gold surface: a new approach. Electrochim. Acta **50**(21), 4283–4288 (2005)
27. M. Manolova, V. Ivanova, D.M. Kolb, H.-G. Boyen, P. Ziemann, M. Büttner, A. Romanyuk, P. Oelhafen, Metal deposition onto thiol-covered gold: platinum on a 4-mercaptopyridine SAM. Surf. Sci. **590**(2-3), 146–153 (2005)
28. M. Manolova, M. Kayser, D.M. Kolb, H.-G. Boyen, P. Ziemann, D. Mayer, A. Wirth, Rhodium deposition onto a 4-mercaptopyridine SAM on Au(111). Electrochim. Acta **52**(8), 2740–2745 (2007)
29. F. Eberle, M. Saitner, H.-G. Boyen, J. Kucera, A. Gross, A. Romanyuk, P. Oelhafen, M. D'Olieslaeger, M. Manolova, D.M. Kolb, A molecular double decker: extending the limits of current metal-molecule hybrid structures. Angew. Chemie - Int. Ed **49**(2), 341–345 (2010)
30. J.A. Keith, T. Jacob, Atomic-level elucidation of the initial stages of self-assembled monolayer metallization and nanoparticle formation. Chem. - A Eur. J. **16**(41), 12381–12386 (2010)
31. J. Kucera, A. Gross, Adsorption of 4-mercaptopyridine on Au(111): a periodic DFT study. Langmuir **24**(24), 13985–13992 (2008)
32. L.-J. Wan, Y. Hara, H. Noda, M. Osawa, Dimerization of sulfur headgroups in 4-mercaptopyridine self-assembled monolayers on Au(111) studied by scanning tunneling microscopy. J. Phys. Chem. B **102**(31), 5943–5946 (1998)
33. L.-J. Wan, H. Noda, Y. Hara, M. Osawa, Effect of solution pH on the structure of a 4-mercaptopyridine monolayer self-assembled on Au(111). J. Electroanal. Chem. **489**(1-2), 68–75 (2000)
34. T. Sawaguchi, F. Mizutani, I. Taniguchi, Direct observation of 4-mercaptopyridine and bis(4-pyridyl) disulfide monolayers on Au(111) in perchloric acid solution using in situ scanning tunneling microscopy. Langmuir **14**(13), 3565–3569 (1998)
35. T. Sawaguchi, F. Mizutani, S. Yoshimoto, I. Taniguchi, Voltammetric and in situ STM studies on self-assembled monolayers of 4-mercaptopyridine, 2-mercaptopyridine and thiophenol on Au(111) electrodes. Electrochim. Acta **45**(18), 2861–2867 (2000)
36. H.-G. Boyen, P. Ziemann, U. Wiedwald, V. Ivanova, D.M. Kolb, S. Sakong, A. Gross, A. Romanyuk, M. Büttner, P. Oelhafen, Local density of states effects at the metal-molecule interfaces in a molecular device. Nat. Mater. **5**(5), 394–399 (2006)
37. A. Chen, J. Lipkowski, electrochemical and spectroscopic studies of hydroxide adsorption at the Au(111) electrode. J. Phys. Chem. B **103**(4), 682–691 (1999)
38. P. Rodriguez, J.M. Feliu, M.T.M. Koper, Unusual adsorption state of carbon monoxide on single-crystalline gold electrodes in alkaline media. Electrochem. Commun. **11**(6), 1105–1108 (2009)
39. B.B. Blizanac, M. Arenz, P.N. Ross, N.M. Marković, Surface electrochemistry of CO on reconstructed gold single crystal surfaces studied by infrared reflection absorption spectroscopy and rotating disk electrode. J. Am. Chem. Soc. **126**(32), 10130–10141 (2004)
40. B.N. Zope, D.D. Hibbitts, M. Neurock, R.J. Davis, Reactivity of the gold/water interface during selective oxidation catalysis. Science **330**(6000), 74–78 (2010)
41. Y. Kwon, S.C.S. Lai, P. Rodriguez, M.T.M. Koper, Electrocatalytic oxidation of alcohols on gold in alkaline media: base or gold catalysis? J. Am. Chem. Soc. **133**(18), 6914–6917 (2011)